nature physics

Article

https://doi.org/10.1038/s41567-023-02250-w

Modulated Kondo screening along magnetic mirror twin boundaries in monolayer MoS_2

Received: 17 October 2022

Accepted: 14 September 2023

Published online: 9 November 2023

Check for updates

Camiel van Efferen [1] ✉, Jeison Fischer [1], Theo A. Costi [2,3], Achim Rosch [4], Thomas Michely [1] & Wouter Jolie [1]

When a single electron is confined to an impurity state in a metal, a many-body resonance emerges at the Fermi energy if the electron bath screens the impurity's magnetic moment. This is the Kondo effect, originally introduced to explain the abnormal resistivity behaviour in bulk magnetic alloys, and it has been realized in many quantum systems over the past decades, ranging from heavy-fermion lattices down to adsorbed single atoms. Here we describe a Kondo system that allows us to experimentally resolve the spectral function consisting of impurity levels and a Kondo resonance in a large Kondo temperature range, as well as their spatial modulation. Our approach is based on a discrete half-filled quantum confined state within a MoS_2 grain boundary, which—in conjunction with numerical renormalization group calculations—enables us to test the predictive power of the Anderson model that is the basis of the microscopic understanding of Kondo physics.

The Kondo effect of single magnetic atoms or molecules on metal surfaces has been the subject of intense research since it was first observed by scanning tunnelling microscopy (STM)[1,2]. Although the Kondo resonance has been well characterized for numerous systems[3,4], the underlying atomic or molecular impurity levels that give rise to it have largely remained experimentally inaccessible. This is due to the dominant contribution of substrate states to the tunnelling current, which lie in the same energy range as the localized *d* and *f* orbitals involved. Furthermore, the strong hybridization of the impurity states with these substrate states—electronvolts away from the Fermi energy—obscures the connection between Kondo resonance and impurity levels. Although STM experiments for magnetic atoms on surfaces show that their behaviour close to the Fermi energy can often be understood in terms of the universal physics of the Kondo effect, the absence of a full characterization of their impurity levels and Coulomb interactions has led to a strong dependence on theoretical input to clarify the origin of the measured signals. For example, the line shapes around zero bias, observed in the STM spectra for Co on noble metal surfaces[1], were considered as paradigms for a Kondo resonance, but have recently been argued to originate from exotic spin excitations rather than the Kondo effect[5]. As a consequence, theoretical predictions for the dependence of the Kondo resonance on energy position, strength of local interactions and width of the impurity level[4,6] could not be tested due to the absence of experimental data.

A promising approach to enable the local detection of impurity levels is to spatially confine electrons, as done in a quantum dot[7–11]. When a confined state at the Fermi energy E_F is filled with a single electron, strong Coulomb repulsion can lift the degeneracy of the energy level, leading to the formation of a singly occupied state below E_F mimicking the half-filled orbital of a magnetic atom. A Kondo resonance emerges when the non-degenerate states couple to an electron bath in close proximity[7,8,11]. The advantages of the confinement approach are a small separation of the non-degenerate states, together with a large spatial extension of the confined wavefunction. In quantum dot systems, these wavefunctions are, however, not accessible due to the lack of spatial resolution. Here we present a system where scanning tunnelling spectroscopy (STS) and STM, with their unsurpassed energy and spatial resolution, can be used to track the Kondo resonance along with the impurity levels and the spatial modulation of their wavefunctions on the atomic scale. It enables us to compare experimental data

[1]II. Physikalisches Institut, Universität zu Köln, Köln, Germany. [2]Peter Grünberg Institut, Forschungszentrum Jülich, Jülich, Germany. [3]Institute for Advanced Simulation, Forschungszentrum Jülich, Jülich, Germany. [4]Institut für Theoretische Physik, Universität zu Köln, Köln, Germany. ✉e-mail: efferen@ph2.uni-koeln.de

https://doi.org/10.1038/s41567-023-02250-w

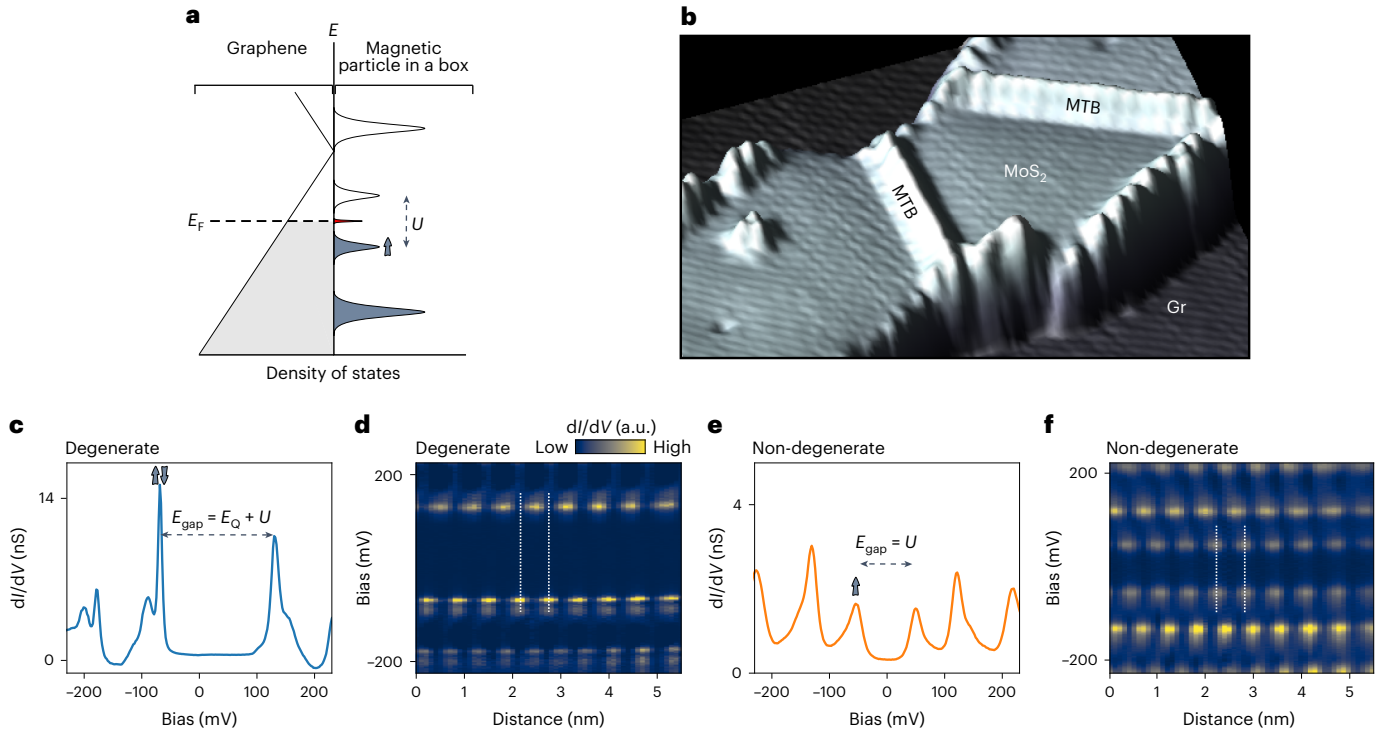

Fig. 1 | Kondo effect within a MoS_2 MTB. a, Kondo coupling of graphene (bath) with the non-degenerate states (impurity) confined along a MoS_2 MTB. Fermi energy E_F and Coulomb energy U are indicated (see the main text). The electron inside the highest occupied state is symbolized by an arrow. **b**, Atomically resolved topography of a single-layer MoS_2 island on graphene, with two MTBs of lengths 7.1 nm (left) and 9.0 nm (right), separating mirror-symmetric domains. **c**,**e**, Spatially averaged d*I*/d*V* spectra along an MTB of 8.6 nm before (**c**) and after (**e**) voltage pulses applied with the STM, being in a state that is either degenerate (**c**) or non-degenerate (**e**). **d**,**f**, Conductance colour maps showing spatially resolved d*I*/d*V* spectra along the MTB. The dashed white lines are added to highlight the phase relation between the states on either side of E_F in the middle of the boundary. STM/STS parameters: for **b**, 20 × 20 nm^2, V_{set} = 500.0 mV, I_{set} = 10 pA; for **c** and **d**, V_{set} = 500.0 mV, I_{set} = 1.0 nA; for **e** and **f**, V_{set} = 500.0 mV, I_{set} = 0.5 nA; V_{mod} = 2.5 mV.

with unsurpassed precision to predictions for the Anderson model of the Kondo effect obtained through numerical renormalization group (NRG) calculations.

Our Kondo system is realized in a MoS_2 mirror twin boundary (MTB), a line defect of finite length that hosts confined states in the bandgap of the semiconducting two-dimensional material[12–14]. Due to its one-dimensional nature, strong Coulomb interactions push the states around the Fermi energy apart and transform higher excitations into the bosonic spin and charge excitations of a confined Tomonaga–Luttinger liquid[14,15]. The lowest-energy excitations of such a system can, however, simply be described by a single fermionic level, which is either empty, singly occupied or doubly occupied. Figure 1a sketches the local density of states around the Fermi energy of an MTB placed on a graphene substrate. The electron bath is represented by graphene's Dirac electrons, which exhibit a linear energy dependence close to the Dirac point[16]. The discrete energy levels sketched in Fig. 1a (right) are quantized states within the one-dimensional MoS_2 MTB. The two energy levels closest to the Fermi energy describe excitations, where a single electron is added to or removed from the MTB. When the highest occupied level is filled by a single electron, the strong Coulomb interaction U prohibits a second electron to enter, creating a spin-$\frac{1}{2}$ system localized along the MTB. This spin couples to the bath and creates a Kondo resonance pinned to E_F through resonant spin-flip processes, as we demonstrate below.

A MoS_2 monolayer island hosting two such MTBs is shown in Fig. 1b. The finite length of the MTBs leads to confined energy levels with a spacing inversely proportional to the length of the wire[14]. When the highest energy level is filled with two electrons, there is no unpaired magnetic moment and hence no Kondo effect. This situation is depicted in Fig. 1c, which displays the averaged differential conductance d*I*/d*V* along an MTB. The d*I*/d*V* signal of the STM is proportional to the local density of states as a function of energy (given by the bias voltage). We find a series of peaks corresponding to quantized energy levels. Satellite peaks attributed to phonon-induced inelastic tunnelling processes are observed at fixed energy intervals of |24.8| ± 3.7 and |47.7| ± 4.1 meV from the main peaks[13]. The peaks closest to E_F exhibit an energy gap of $E_{gap} = E_Q + U$, where E_Q is the confinement energy and U is the Coulomb energy 'penalty' incurred due to strong Coulomb interactions[14,17]. The standing waves corresponding to the energy levels closest to E_F are mapped in Fig. 1d using a series of d*I*/d*V* spectra taken along the MTB. These standing waves are out of phase in the centre of the boundary, as expected for successive degenerate particle-in-a-box states (Supplementary Note 1)[14].

The number of electrons within an MTB can be tuned with the help of the STM, either continuously with a back gate or stepwise via voltage pulses in the range of $|V_{pulse}| = |1.0–2.5|$ eV (Supplementary Note 2), as demonstrated previously for the isostructural two-dimensional material $MoSe_2$ (refs. 17,18). Figure 1e shows the spectrum obtained on the same boundary after such a voltage pulse. The gap at E_F is now reduced to the pure Coulomb energy U, splitting the formerly degenerate energy level at the Fermi energy. The splitting leads to a singly occupied state below E_F that is energetically separated from the doubly occupied state by U, which is the unoccupied state visible just above E_F in the single-electron picture. In the spatially resolved series of d*I*/d*V* spectra (Fig. 1f), the non-degenerate nature of the energy levels closest to E_F is visible as an in-phase beating of the two standing waves above and below the Fermi energy, which would collapse to a degenerate standing wave without Coulomb interaction U.

https://doi.org/10.1038/s41567-023-02250-w

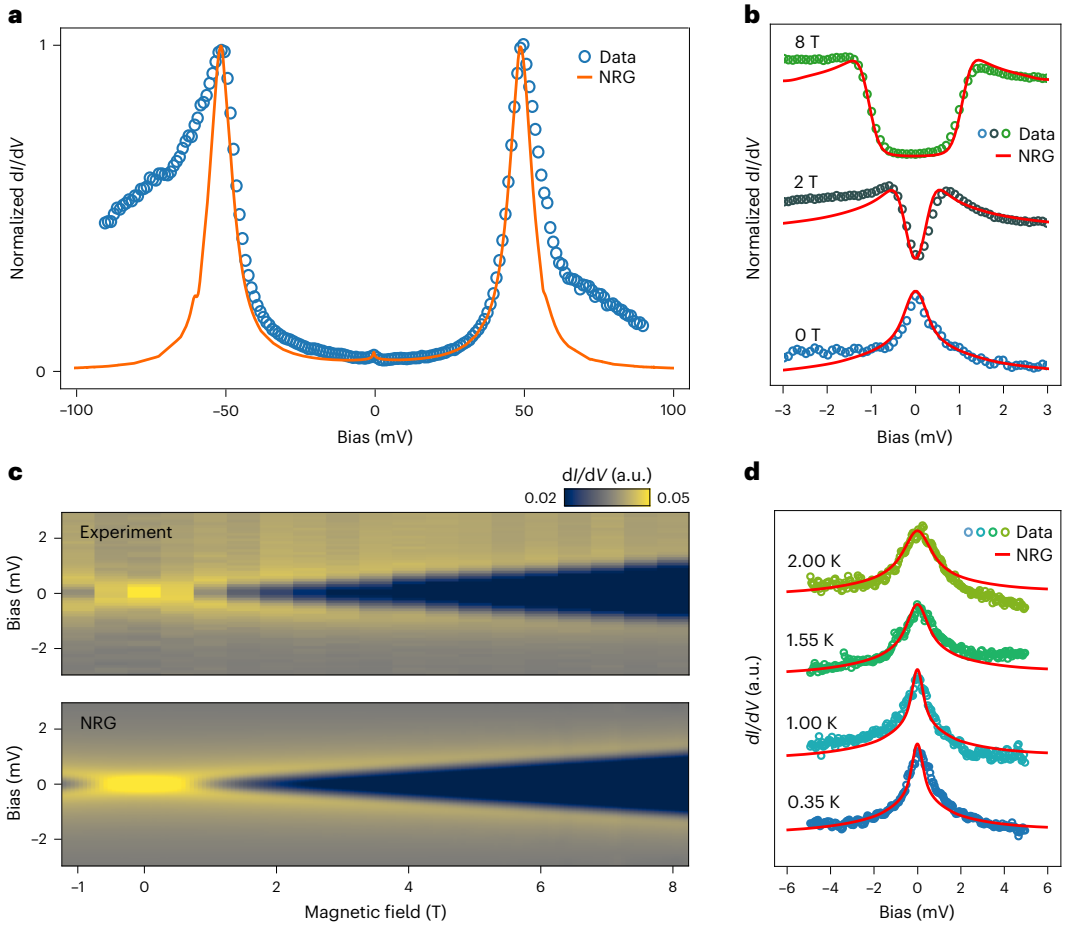

Fig. 2 | Kondo resonance and NRG simulation of magnetic MTB at different magnetic fields and temperatures. a, dI/dV spectrum of the impurity level with Kondo resonance (blue circles; L = 8.6 nm, ε = −51.00 meV, U = 100.00 meV, γ = 10.40 meV) and the corresponding NRG simulation (orange line; ε = −51.00 meV, U = 100.00 meV, γ_{NRG} = 9.35 meV). Experimental spectra and theory are normalized to the non-degenerate states. The NRG curves have been broadened by the experimental resolution. **b**, dI/dV spectra of Kondo resonance at different magnetic fields (coloured circles) with NRG simulation (red line). Data are plotted in the same scale as **a**. **c**, Conductance (dI/dV signal) colour maps of the Kondo resonance as a function of bias and magnetic field, comparing the experimental spectra (top) and NRG simulation (bottom) with g = 2.5. **d**, Dependence of the dI/dV signal on temperature with the NRG simulation. STM/STS parameters: for **a**, V_{set} = 90.0 mV, I_{set} = 1.0 nA, V_{mod} = 1.0 mV; for **b** and **c**, V_{set} = 10.0 mV, I_{set} = 1.0 nA, V_{mod} = 0.2 mV; for **d**, V_{set} = 5.0 mV, I_{set} = 1.0 nA, V_{mod} = 0.2 mV.

In between the two non-degenerate states, a narrow zero-bias peak (ZBP) is found in the dI/dV spectra (Fig. 2a,b). The ZBP shows a relatively low intensity compared with the non-degenerate peaks (Fig. 2a), but becomes well visible when the tip–sample distance is reduced (Fig. 2b). No substantial change in width and height (relative to the background signal) of the ZBP is observed when varying the tip–sample distance (Supplementary Note 3), whereas its intensity quickly decays away from the MTB (Supplementary Note 4). To understand the nature of the ZBP, we investigate the influence of magnetic fields and temperature on the shape of the ZBP (Fig. 2b–d). We find a clear Zeeman splitting of the ZBP with increasing magnetic field (Fig. 2b,c), whereas the ZBP broadens when the temperature is increased (Fig. 2d), in line with the expectation for a Kondo resonance[4].

Theoretically, such a Kondo system is described by the Anderson model, which is established for a single-impurity level coupled to an electron bath[19]. The dI/dV spectrum of this model is simulated using the NRG theory and compared with the experimental spectrum (Fig. 2a). The NRG simulation resembles the experimental spectrum with striking accuracy for both high- and low-energy features. This agreement is highlighted when comparing the magnetic-field dependence shown for an individual spectrum (Fig. 2b) and as a colour plot (Fig. 2c). In both experiment and theory, the resonance transforms into a pronounced gap at high magnetic fields. From the splitting of the Kondo resonance with an out-of-plane magnetic field B, we extract a g-factor of g = 2.5. A smaller splitting is observed for in-plane fields (Supplementary Note 5). An excellent match between experiment and theory is also found in the temperature dependence of the Kondo resonance (Fig. 2d and Supplementary Note 6). Note that no additional fitting was performed to obtain the spectra in Fig. 2b–d, with the experimental magnetic field and temperature used simply as an input for NRG calculations.

The Anderson model parameters required for these simulations are the splitting U of the non-degenerate states, position ε of the impurity orbital relative to the Fermi energy and bare width γ_0 of the impurity level (Supplementary Note 7). The first two are directly obtained from the experiment (Fig. 3a). A crucial point concerns the extraction of γ_0 from the measured width γ. First, as pointed out earlier[20], spin-flip processes in the Kondo regime increase the experimentally observable width γ of the non-degenerate peaks at ε and $\varepsilon + U$ by a factor of two, that is, $\gamma = 2\gamma_0$ (Supplementary Note 8). Second, the broad inelastic tail related to phonons leads to a systematic overestimation of the experimental γ, which we counteract by fitting the inner tail of the non-degenerate peaks (Supplementary Notes 9 and 11). Taking this into account, we find agreement on a quantitative level between experiment and theory. Importantly, NRG is able to fully predict the magnetic field

https://doi.org/10.1038/s41567-023-02250-w

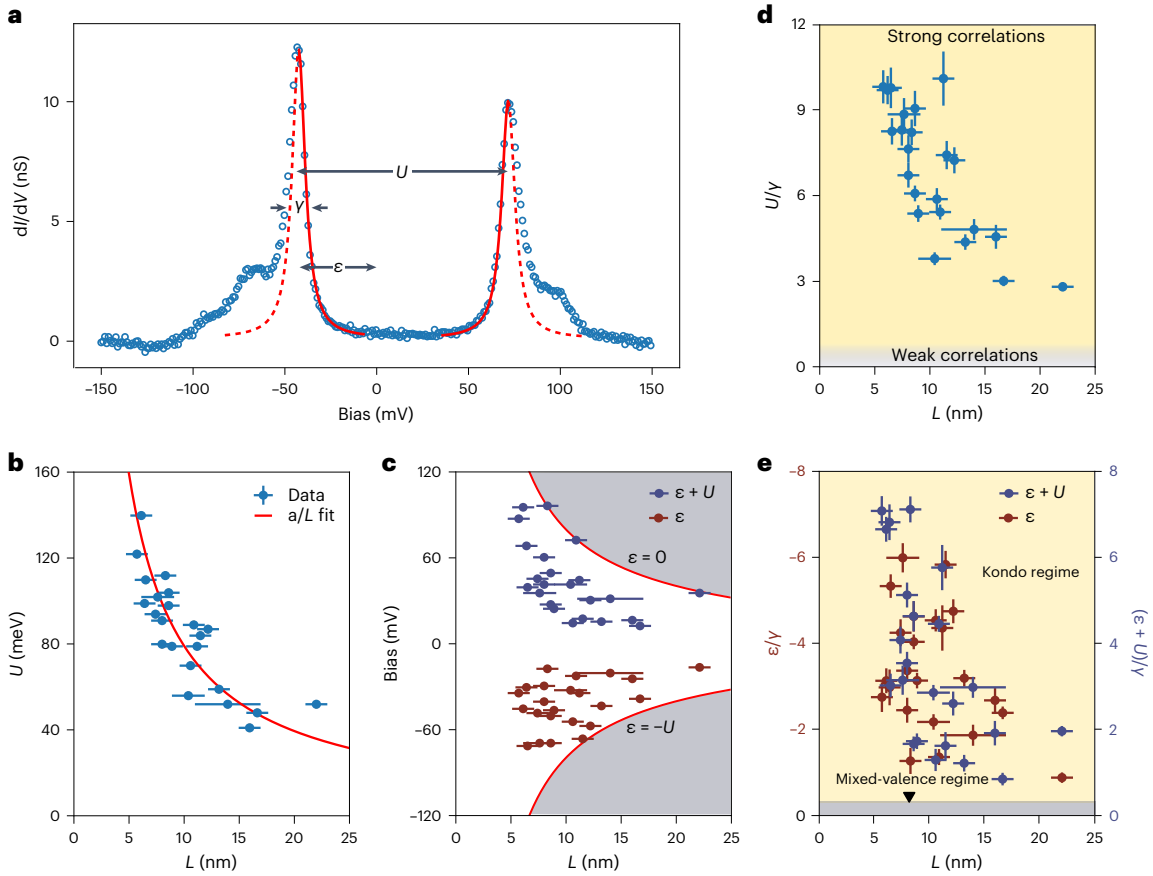

Fig. 3 | Tuning the Kondo effect and correlations. a, dI/dV spectrum of non-degenerate states (blue circles) of an MTB with L = 6.5 nm, ε = −39.0 meV, U = 110.0 meV, γ = 10.8 meV. Coulomb energy U, energy spacing ε from E_F, and full-width at half-maximum of the main Lorentzian peak γ are indicated, defining the parameters needed for an NRG simulation. Lorentzian functions fitted to the inner slope of the peaks are shown, from which the full-width at half-maximum γ is extracted. **b**, Coulomb gap (U) for MTBs of different lengths (L). The a/L fit gives a = 793 meV nm = $0.55e^2/(4\pi\varepsilon_0)$, where e is the electron charge. **c**, Peak position of non-degenerate states below (ε) and above ($\varepsilon + U$) the Fermi energy. As L increases, the gap U between the states shrinks. **d**, Correlation strength U/γ of MTBs, calculated for MTBs with U and γ obtained from Lorentzian fits. **e**, Peak position of the non-degenerate states in units of γ. For all the boundaries, $|\varepsilon| \geq \gamma/4$ and $|\varepsilon + U| \geq \gamma/4$, placing them in the Kondo regime. Each data point for U, ε or γ represents the value extracted from a Lorentzian fit to the spectra, with a minimum error corresponding to the experimental resolution, whereas the errors in L are based on the accuracy with which we were able to determine the particular length of a boundary. STM/STS parameters: for **a**, V_{set} = 200 mV, I_{set} = 0.2 nA, V_{mod} = 1.0 mV. All the spectra used in **b**–**e** were measured with V_{mod} = 1.0 mV, but under different stabilization voltages and currents.

and temperature dependence of the experimental Kondo resonance purely based on parameters stemming from the impurity level.

Having the capability to predict properties of the Kondo effect using information on the impurity states, we make use of the latter to demonstrate the high tunability of our Kondo system by extracting the parameters (U, ε, γ) for 23 different MTBs of varying length L. We find a clear inverse length dependence of U (Fig. 3b), which is a consequence of the lower Coulomb energy of electrons when they are spread over a larger L (Supplementary Note 10). A fit $\widetilde{U}(L) = a/L$ is shown in Fig. 3b (solid line). Strong variations are found in ε, which can fluctuate between $-U$ and the Fermi energy. This energy range is visualized in Fig. 3c using the fit function $\widetilde{U}(L)$ (Fig. 3b). The scatter in γ, which shows no indication of a length dependence (Supplementary Note 11), is most probably related to the large momentum mismatch of electrons in the MTB and in graphene. This mismatch suppresses direct tunnelling and enhances the role of defect-induced tunnelling processes.

With the knowledge of (U, ε, γ), we first point out that all our non-degenerate states cover a wide range of the strongly correlated regime, that is, $U/\gamma \gg 1/2$ (Fig. 3d). Furthermore, all these boundaries satisfy $-\varepsilon/\gamma \gg 1/4$ and $(\varepsilon + U)/\gamma \gg 1/4$, showing that these systems are in the Kondo regime (Fig. 3e and Supplementary Note 7). The realization of a wide range of level energies ε and Coulomb repulsions U in these boundaries translates into a wide range of Kondo temperatures, namely, $T_K = 10^{-10}$ to 10^{-4} K, where $k_B T_K = w\gamma_0\sqrt{U/4\gamma_0}\exp(-\pi|\varepsilon||\varepsilon + U|/\gamma_0 U)$ and w = 0.4128 is the Wilson number (Supplementary Note 12). Such small Kondo temperatures are consistent with the small density of states of the substrate and the large van der Waals gap between the substrate and MoS_2. Since we have access to the microscopic parameters (U, ε, γ), T_K is directly calculated and we do not require the estimates of Kondo coupling to extract T_K. Supplementary Note 12 provides the calculation of Kondo couplings. These results highlight that there is strong internal tunability of the Kondo effect in MoS_2 MTBs. Without the need to change the dielectric or chemical environment, a wide range of Kondo temperatures is immediately available due to the wide range of boundary lengths and the asymmetry of the states with respect to the Fermi energy.

Finally, we investigated the spatial distribution of the Kondo resonance together with the non-degenerate states along an MTB. The non-degenerate states beat along the MTB with a wavelength related to their Fermi wavevector[14,18,21], as expected for a particle in a box. This beating is apparent in the topograph shown in Fig. 4a. Focusing on the two maxima in the boxed area in Fig. 4a, the set of dI/dV spectra taken along the MTB (Fig. 4b) shows the beating of the two non-degenerate states on either side of E_F. The two states are in phase along the MTB

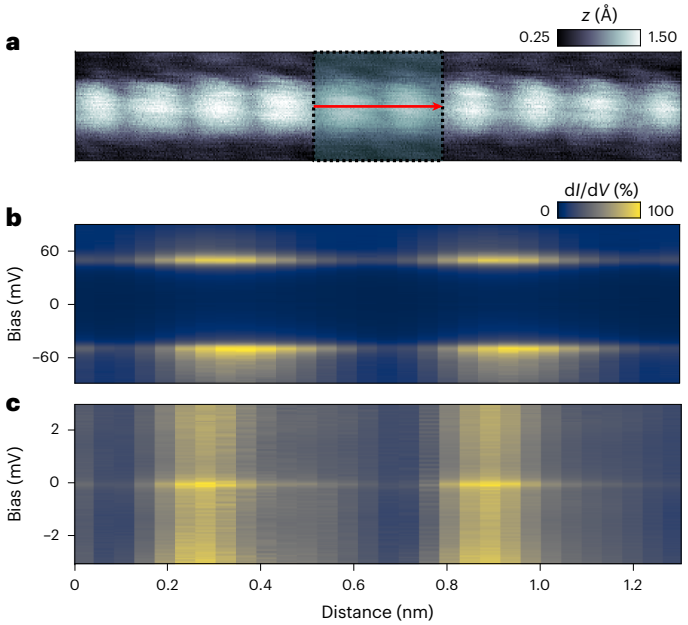

Fig. 4 | Modulated Kondo screening along the particle in a box. a, Topography along an MTB of $L = 8.6$ nm, $\varepsilon = -51.00$ meV, $U = 100.00$ meV, $\gamma = 9.35$ meV, showing the electronic beating of the confined state near E_F. The red arrow indicates where the spectra shown in **b** and **c** were taken. **b**, Conductance colour map of the constant-height d*I*/d*V* spectra of the non-degenerate peaks along the MTB. **c**, Conductance colour map showing the constant-height d*I*/d*V* spectra of the Kondo resonance along the same path. STM/STS parameters: for **a**, $6.0 \times 1.1\ \mathrm{nm}^2$, $V_{set} = -10.0$ mV, $I_{set} = 5$ pA; for **b**, $V_{set} = 90.0$ mV, $V_{mod} = 1.0$ mV; for **c**, $V_{set} = 10$ mV, $V_{mod} = 0.2$ mV. $I_{set} = 0.5$ nA for all the spectra.

as they are derived from the same energy level, which is split due to a Coulomb interaction. The d*I*/d*V* line scan shown in Fig. 4c, taken at the same location, shows the Kondo resonance. The amplitude of the Kondo resonance beats in phase with the non-degenerate peaks (compare Fig. 4b). In particular, we find that the amplitude of the resonance is linearly dependent on the peak amplitude of the MTB states, emphasizing the direct relation between these elements of the Kondo effect. These results are reminiscent of the orbital symmetries observed in Shiba states on superconductors, which were attributed to anisotropic scattering due to the orbital shapes of the magnetic atom[22,23]. We envision that using extended magnetic wavefunctions like those of the MTBs might enable direct access to the correlated behaviour of Shiba states and wavefunction, as observed here for the Kondo effect.

As for the correspondence between the Anderson model and experiment, further refining of the model, although outside the scope of this paper, can be envisioned. In particular, as the theoretical model does not include phonons, the inelastic tails and phonon side peaks of the high-energy peaks (Fig. 3a) are not taken into account. The experimental peaks also slightly vary in height and width, which may arise from the bias dependence of the density of states neglected within our model (the Fermi energy of our graphene layer is estimated to lie 250 meV from the Dirac point[24], a substantially larger range than the energy scales relevant for our experiment). Spin–orbit interactions are, furthermore, expected to induce an anisotropic magnetic response, whereas multichannel effects arising from virtual transitions to other high-energy states of the MTB are also neglected in the current approach.

In summary, we established one-dimensional magnetic MTBs in a two-dimensional material as a prototypical system to characterize the Kondo effect. We presented a comprehensive study of a fully accessible spin-$\frac{1}{2}$ Kondo system allowing us not only to characterize the Kondo resonance itself but also to quantitatively determine the impurity levels. We find that NRG calculations accurately reproduce the intensity, shape, magnetic field and temperature dependence of the Kondo resonance when simulating the impurity states. By quantitatively relating the high- and low-energy features, our experiment confirms many properties of the Anderson model both qualitatively and quantitatively. This includes the ratio of amplitudes of high- and low-energy peaks and an extra broadening of the high-energy peaks by a factor 2 due to spin-flip processes. In addition, our system reveals the real-space relation between the impurity-level wavefunction and the spatial dimension of the Kondo resonance. The variability of the parameters U (via boundary length), ρ (via doping[25]) and ε (via pulsing or gating) makes MTBs in transition metal dichalcogenides a valuable testbed for nanoscale magnetic investigations. Controlled coupling of the extended magnetic wavefunction to localized magnetic defects[26] or adatoms represent exciting perspectives.

Online content

Any methods, additional references, Nature Portfolio reporting summaries, source data, extended data, supplementary information, acknowledgements, peer review information; details of author contributions and competing interests; and statements of data and code availability are available at https://doi.org/10.1038/s41567-023-02250-w.

References

1. Madhavan, V., Chen, W., Jamneala, T., Crommie, M. F. & Wingreen, N. S. Tunneling into a single magnetic atom: spectroscopic evidence of the Kondo resonance. *Science* **280**, 567–569 (1998).
2. Li, J., Schneider, W. D., Berndt, R. & Delley, B. Kondo scattering observed at a single magnetic impurity. *Phys. Rev. Lett.* **80**, 2893–2896 (1998).
3. Ternes, M., Heinrich, A. J. & Schneider, W.-D. Spectroscopic manifestations of the Kondo effect on single adatoms. *J. Phys.: Condens. Matter* **21**, 053001 (2008).
4. Ternes, M. Spin excitations and correlations in scanning tunneling spectroscopy. *New J. Phys.* **17**, 063016 (2015).
5. Bouaziz, J., Mendes Guimarães, F. S. & Lounis, S. A new view on the origin of zero-bias anomalies of Co atoms atop noble metal surfaces. *Nat. Commun.* **11**, 6112 (2020).
6. Schrieffer, J. R. & Wolff, P. A. Relation between the Anderson and Kondo Hamiltonians. *Phys. Rev.* **149**, 491–492 (1966).
7. Goldhaber-Gordon, D. et al. Kondo effect in a single-electron transistor. *Nature* **391**, 156–159 (1998).
8. Cronenwett, S. M., Oosterkamp, T. H. & Kouwenhoven, L. P. A tunable Kondo effect in quantum dots. *Science* **281**, 540–544 (1998).
9. De Franceschi, S. et al. Out-of-equilibrium Kondo effect in a mesoscopic device. *Phys. Rev. Lett.* **89**, 156801 (2002).
10. Leturcq, R. et al. Probing the Kondo density of states in a three-terminal quantum ring. *Phys. Rev. Lett.* **95**, 126603 (2005).
11. Borzenets, I. V. et al. Observation of the Kondo screening cloud. *Nature* **579**, 210–213 (2020).
12. Liu, H. et al. Dense network of one-dimensional midgap metallic modes in monolayer $MoSe_2$ and their spatial undulations. *Phys. Rev. Lett.* **113**, 066105 (2014).
13. Barja, S. et al. Charge density wave order in 1D mirror twin boundaries of single-layer $MoSe_2$. *Nat. Phys.* **12**, 751–756 (2016).
14. Jolie, W. et al. Tomonaga-Luttinger liquid in a box: electrons confined within MoS_2 mirror-twin boundaries. *Phys. Rev. X* **9**, 11055 (2019).
15. Ma, Y. et al. Angle resolved photoemission spectroscopy reveals spin charge separation in metallic $MoSe_2$ grain boundary. *Nat. Commun.* **8**, 14231 (2017).
16. Castro Neto, A. H., Guinea, F., Peres, N. M. R., Novoselov, K. S. & Geim, A. K. The electronic properties of graphene. *Rev. Mod. Phys.* **81**, 109–162 (2009).

17. Yang, X. et al. Manipulating Hubbard-type Coulomb blockade effect of metallic wires embedded in an insulator. *Natl Sci. Rev.* **10**, nwac210 (2022).
18. Zhu, T. et al. Imaging gate-tunable Tomonaga–Luttinger liquids in 1H-$MoSe_2$ mirror twin boundaries. *Nat. Mater.* **21**, 748–753 (2022).
19. Anderson, P. W. A poor man's derivation of scaling laws for the Kondo problem. *J. Phys. C: Solid State Phys.* **3**, 2436–2441 (1970).
20. Logan, D. E., Eastwood, M. P. & Tusch, M. A. A local moment approach to the Anderson model. *J. Phys.: Condens. Matter* **10**, 2673 (1998).
21. Yang, K. et al. Probing resonating valence bond states in artificial quantum magnets. *Nat. Commun.* **12**, 993 (2021).
22. Ruby, M., Peng, Y., von Oppen, F., Heinrich, B. W. & Franke, K. J. Orbital picture of Yu-Shiba-Rusinov multiplets. *Phys. Rev. Lett.* **117**, 186801 (2016).
23. Choi, D. J. et al. Building complex Kondo impurities by manipulating entangled spin chains. *Nano Lett.* **17**, 6203–6209 (2017).
24. Ehlen, N. et al. Narrow photoluminescence peak of epitaxial MoS_2 on graphene/Ir(111). *2D Mater.* **6**, 011006 (2019).
25. van Efferen, C. et al. Metal-insulator transition in monolayer MoS_2 via contactless chemical doping. *2D Mater.* **9**, 025026 (2022).
26. Cochrane, K. A. et al. Spin-dependent vibronic response of a carbon radical ion in two-dimensional WS_2. *Nat. Commun.* **12**, 7287 (2021).

Methods

The MoS_2 monolayers were grown in situ on a graphene substrate, supported by an Ir(111) crystal, in a preparation chamber with base pressure $p < 5 \times 10^{-10}$ mbar. Ir(111) is cleaned by 1.5 keV Ar^+-ion erosion and annealing to temperatures of $T \approx 1{,}550$ K. Graphene is grown on Ir(111) by two steps. First, room-temperature ethylene exposure till saturation followed by 1,370 K thermal decomposition gives well-oriented graphene islands. Second, exposure to 2,000 L ethylene at 1,370 K for 600 s yields a complete single-crystal graphene layer[27]. Monolayer MoS_2 is grown by Mo deposition in an elemental S pressure of 7×10^{-9} mbar (ref. 28). Subsequently, the sample is annealed to 1,050 K in the same S background pressure.

STM and STS are carried out at a base operating temperature of $T = 0.35$ K after in situ transfer from the preparation chamber. STS is performed with the lock-in technique, at a modulation frequency of 907.0 Hz. STM images are taken in the constant-current mode. Some of the data shown in Fig. 3d were taken using a second STM with an operating temperature of $T = 6.5$ K.

We briefly outline the NRG procedure for the Anderson impurity model. The details are provided elsewhere[29–32]. In short, the NRG consists of iteratively diagonalizing the following equivalent linear chain form of the Anderson impurity model (equation (1) and Supplementary Note 7):

$$H = \sum_{\sigma} \varepsilon_{\sigma} n_{\sigma} + U n_{\uparrow} n_{\downarrow} + V \sum_{\sigma} \left(f_{0\sigma}^{\dagger} d_{\sigma} + \text{h.c.} \right) + \sum_{n=0}^{\infty} \sum_{\sigma} t_n \left(f_{n\sigma}^{\dagger} f_{n+1\sigma} + \text{h.c.} \right), \quad (1)$$

where $\varepsilon_{\sigma} = \varepsilon - g\mu_B B\sigma/2$ is the impurity-level energy for spin σ measured relative to the Fermi energy, B is a local magnetic field, U is the Coulomb repulsion and $\gamma_0 = 2\pi\rho V^2$ is the hybridization strength for conduction electron density of states ρ. The iterative diagonalization is carried out on a sequence of decreasing energy scales $t_n \approx D\Lambda^{-n/2}$, where $n = 0, 1\ldots$, with discretization parameter $\Lambda > 1$, by diagonalizing successive truncated Hamiltonians H_N ($N = 0, 1\ldots$) conduction electron orbitals $f_{n\sigma}$ ($n = 0\ldots N$) using the recursion relation $H_{N+1} = H_N + t_N \sum_{\sigma} (f_{N\sigma}^{\dagger} f_{N+1\sigma} + \text{h.c.}) \equiv \mathcal{T}[H_N]$. This procedure yields the many-body eigenvalues and eigenvectors as well as the matrix elements of physical observables of interest. The logarithmic discretization parameter $\Lambda > 1$ separates out the many (infinite) energy scales of the conduction band, from high energies (small n) to intermediate energies (intermediate n) and low energies ($n \gg 1$), allowing the physics to be iteratively obtained on each successive energy scale. This non-perturbative approach allows essentially exact calculations for thermodynamical and dynamical quantities, including the spectral function, to be carried out on all the temperature and energy scales. In fitting the calculated $\mathrm{d}I/\mathrm{d}V$ to experiment, a constant elastic background of less than 1% of the total intensity takes into account direct tunnelling from the substrate.

To compare NRG with experiment (Supplementary Note 13), it is important to take the experimental broadening due to temperature and lock-in modulation into account. Experimentally, we use an oscillating voltage with an amplitude of $V_{\text{mod}} = 0.2$ mV, $V(t) = V_0 + V_{\text{mod}}\cos(\omega t)$. As the experimental differential conductance (proportional to $A(\omega)$) is obtained from the standard lock-in technique, we obtain a spectral function $A(\omega)$ broadened by the experimental resolution from $\tilde{A}(V_0) = \frac{1}{2TV_{\text{mod}}} \int_0^T \mathrm{d}t \cos(\omega t) \int_0^{V(t)} A(\omega)\mathrm{d}\omega$. Concerning the temperature implemented in NRG, we use the experimental temperature. At or below 0.7 K, a constant $T_{\text{eff}} = 0.7$ K is implemented, which is equal to the temperature of the tunnel junction measured at the lowest experimental temperatures[33].

Data availability

All experimental and simulated data in the Article are available via Zenodo at https://doi.org/10.5281/zenodo.8296778 (ref. 34). Further data are available from the corresponding author on reasonable request. Source data are provided with this paper.

Code availability

Code that supports the plots within this paper and other findings of this study are available from the corresponding author upon reasonable request.

References

27. Coraux, J. et al. Growth of graphene on Ir(111). *New J. Phys.* **11**, 023006 (2009).
28. Hall, J. et al. Molecular beam epitaxy of quasi-freestanding transition metal disulphide monolayers on van der Waals substrates: a growth study. *2D Mater.* **5**, 025005 (2018).
29. Wilson, J., Di Salvo, F. & Mahajan, S. Charge-density waves and superlattices in the metallic layered transition metal dichalcogenides. *Adv. Phys.* **24**, 117–201 (1975).
30. Krishna-murthy, H. R., Wilkins, J. W. & Wilson, K. G. Renormalization-group approach to the Anderson model of dilute magnetic alloys. I. Static properties for the symmetric case. *Phys. Rev. B* **21**, 1003–1043 (1980).
31. Bulla, R., Costi, T. A. & Pruschke, T. Numerical renormalization group method for quantum impurity systems. *Rev. Mod. Phys.* **80**, 395–450 (2008).
32. Hewson, A. C. *The Kondo Problem to Heavy Fermions* (Cambridge Univ. Press, 1997).
33. Bagchi, M., Brede, J. & Ando, Y. Observability of superconductivity in Sr-doped Bi_2Se_3 at the surface using scanning tunneling microscope. *Phys. Rev. Mater.* **6**, 034201 (2022).
34. van Efferen, C. Modulated Kondo screening along magnetic mirror twin boundaries in monolayer MoS_2. *Zenodo* https://doi.org/10.5281/zenodo.8296778 (2023).

Acknowledgements

This work was funded by the Deutsche Forschungsgemeinschaft (DFG, German Research Foundation)—project number 277146847–CRC 1238 (subprojects A01, B06 and C02). J.F. acknowledges financial support from the DFG SPP 2137 (Project FI 2624/1-1) T.A.C. gratefully acknowledges the computing time granted through JARA on the supercomputer JURECA at Forschungszentrum Jülich.

Author contributions

W.J. designed the experiments. C.v.E., J.F. and W.J. carried out the measurements. C.v.E. performed most of the analysis of the experimental data under the supervision of W.J. T.A.C. performed the NRG calculations and both T.A.C. and A.R. gave the theoretical input. C.v.E., W.J. and T.M. mainly wrote the manuscript, with help from all the authors. All authors contributed to the discussion and interpretation of the results.

Funding

Open access funding provided by Universität zu Köln.

Competing interests

The authors declare no competing interests.

Additional information

Supplementary information The online version contains supplementary material available at https://doi.org/10.1038/s41567-023-02250-w.

Correspondence and requests for materials should be addressed to Camiel van Efferen.

Peer review information *Nature Physics* thanks Barbara Jones, Rodolfo Miranda and the other, anonymous, reviewer(s) for their contribution to the peer review of this work.